

Pressure-induced phase transition and electronic structure evolution in layered semimetal $HfTe_2$

Mei-Guang Zhang(张美光), Lei Chen(陈磊), Long Feng(冯龙), Huan-Huan Tuo(拓换换),Yun Zhang(张云), Qun Wei(魏群), and Pei-Fang Li(李培芳)

Citation: Chin. Phys. B, 2023, 32 (**8**): 086101. DOI: 10.1088/1674-1056/acd2bf
Journal homepage: http://cpb.iphy.ac.cn; http://iopscience.iop.org/cpb

What follows is a list of articles you may be interested in

Pressure-induced novel structure with graphene-like boron-layer in titanium monoboride

Yuan-Yuan Jin(金园园), Jin-Quan Zhang(张金权), Shan Ling(凌山), Yan-Qi Wang(王妍琪), Song Li(李松), Fang-Guang Kuang(匡芳光), Zhi-Yan Wu(武志燕), and Chuan-Zhao Zhang(张传钊)

Chin. Phys. B, 2022, 31 (**11**): 116104. DOI: 10.1088/1674-1056/ac9222

Pressure-induced phase transition in transition metal trifluorides

Peng Liu(刘鹏), Meiling Xu(徐美玲), Jian Lv(吕健), Pengyue Gao(高朋越), Chengxi Huang(黄呈熙), Yinwei Li(李印威), Jianyun Wang(王建云), Yanchao Wang(王彦超), and Mi Zhou(周密)

Chin. Phys. B, 2022, 31 (**10**): 106104. DOI: 10.1088/1674-1056/ac5887

High-pressure-induced phase transition in cinchomeronic acid polycrystalline form-I

Ting-Ting Yan(颜婷婷), Dong-Yang Xi(喜冬阳), Jun-Hai Wang(王俊海), Xu-Feng Fan(樊旭峰), Ye Wan(万晔), Li-Xiu Zhang(张丽秀), Kai Wang(王凯)

Chin. Phys. B, 2019, 28 (**1**): 016104. DOI: 10.1088/1674-1056/28/1/016104

Room-temperature strong coupling between dipolar plasmon resonance in single gold nanorod and two-dimensional excitons in monolayer WSe_2

Jinxiu Wen(温锦秀), Hao Wang(汪浩), Huanjun Chen(陈焕君), Shaozhi Deng(邓少芝), Ningsheng Xu(许宁生)

Chin. Phys. B, 2018, 27 (**9**): 096101. DOI: 10.1088/1674-1056/27/9/096101

Band engineering of double-wall Mo-based hybrid nanotubes

Lei Tao(陶蕾), Yu-Yang Zhang(张余洋), Jiatao Sun(孙家涛), Shixuan Du(杜世萱), Hong-Jun Gao(高鸿钧)

Chin. Phys. B, 2018, 27 (**7**): 076104. DOI: 10.1088/1674-1056/27/7/076104

Pressure-induced phase transition and electronic structure evolution in layered semimetal $HfTe_2$

Mei-Guang Zhang(张美光)[1,†], Lei Chen(陈磊)[1], Long Feng(冯龙)[1], Huan-Huan Tuo(拓换换)[1], Yun Zhang(张云)[1], Qun Wei(魏群)[2,‡], and Pei-Fang Li(李培芳)[3]

[1] *College of Physics and Optoelectronic Technology, Collaborative Innovation Center of Rare-Earth Functional Materials and Devices Development, Baoji University of Arts and Sciences, Baoji* 721016, *China*
[2] *School of Physics, Xidian University, Xi'an* 710071, *China*
[3] *College of Mathematics and Physics, Inner Mongolia Minzu University, Tongliao* 028043, *China*

(Received 17 March 2023; revised manuscript received 17 April 2023; accepted manuscript online 5 May 2023)

Motivated by the recent experimental work, the pressure-induced structural transition of well-known two-dimensional (2D) $1T$-$HfTe_2$ was investigated up to 50 GPa through the advanced CALYPSO structure search technique combined with the first-principles calculations. Our calculations suggested that the $1T$-$HfTe_2$ will first transform to $C2/m$ phase at 3.6 GPa with a volume reduction of 7.6% and then to $P\bar{6}2m$ phase at 9.6 GPa with a volume collapse of 4.6%. The occurrences of 3D $C2/m$ and $P\bar{6}2m$ phases mainly originated from the enhanced Te–Te interlayer coupling and the drastic distortions of Hf–Te polyhedrons in $P\bar{3}m1$ phase under compression. Concomitantly, the coordination number of Hf atoms increased from six in $P\bar{3}m1$ to eight in $C2/m$ and eventually to nine in $P\bar{6}2m$ at elevated pressure. The metallic and semimetallic nature of $C2/m$ and $P\bar{6}2m$ phases were characterized, and the evidence of the reinforced covalent interactions of Te–Hf and Te–Te orbitals in these two novel high-pressure phases were manifested by the atom-projected electronic DOS and Bader charge.

Keywords: transition metal dichalcogenides, pressure-induced phase transition, crystal structure, electronic structure

PACS: 61.50.Ah, 61.50.Ks, 71.20.–b, 71.18.+y **DOI:** 10.1088/1674-1056/acd2bf

1. Introduction

Layered transition metal dichalcogenides (TMDs) have recently gained intense attention for their varietal structural polymorphs, extraordinary electronic and optical properties as well as potential applications in two-dimensional (2D) devices.[1–6] In particular, more and more interests have been paid to the Hafnium dichalcogenides HfX_2 (X = S, Se, and Te), a typical group of layered TMDs with exotic electronic structures, showing an important application in optoelectronic and electronic.[7–10] HfX_2 adopts the well-known $1T$ trigonal structure ($P\bar{3}m1$, $Z = 1$), consisting of the X–Hf–X sandwich layers along the c-axis direction with weak van der Waals (vdW) interactions.[11] Both HfS_2 and $HfSe_2$ have been manifested to be narrow band-gap semiconductors and possessed higher electron mobility and current density, which make they are favorable candidates for high performance field-effect transistor components, optoelectronic devices, and photovoltaic cells.[12–15] By contrast, $1T$-$HfTe_2$ holds a semimetallic electronic character, with the coexisting electrons and holes bands crossing the Fermi level and strong orbital mixing of Te-p and Hf-d, leading to a large and nonsaturating magnetoresistance.[11,16]

High-pressure is considered as a powerful tool for identifying novel behaviors of solids,[17] as pressure can significantly shorten the distance between atoms and alter their interatomic interactions and electronic bonding states, thus modifying the related physical properties and/or inducing structural phase transitions. Apart from the external electric field and the control of the thickness of the samples,[18–21] the application of pressure or strain has been demonstrated to be a desirable and clean approach in recent experimental and theoretical efforts to modify the structural framework and associated electronic properties of layered TMDs. Different pressure-induced properties of bulk TMDs have been reported, such as the band inversion and the resulting topological phase transition of $TiTe_2$ under pressure,[22] pressure-driven superconductivity in VSe_2 after the suppression of charge density wave (CDW),[23] the reduction of magnetoresistance in WTe_2 upon compression,[24] structural transformation accompanied with metallization in MoS_2, $TiSe_2$, $MoTe_2$, etc.[25–27] For $1T$-HfX_2 compounds, the high-pressure behavior of HfS_2 has been investigated by various works,[28–30] among which Dai and Hu *et al.*[30] had reported that two structural transformations and metallization of HfS_2 occurred at 8.2 GPa, 17.2 GPa and 23.1 GPa, confirmed by the various experimental measurements coupled with first-principles calculations. Combined with various experimental techniques including Raman spectra, optical absorption and resistance measurements as well as

†Corresponding author. E-mail: zhmgbj@126.com
‡Corresponding author. E-mail: weiqunn@xidian.edu.cn

© 2023 Chinese Physical Society and IOP Publishing Ltd

x-ray diffraction (XRD), pressure-driven metallization and superconductivity in $HfSe_2$ have been revealed in recent experimental works.[31–33] Two independent experimental works executed by Li *et al.*[31] and Huang *et al.*[32] found that the 1*T*-$HfSe_2$ transformed to a monoclinic $C2/m$ intermediate structure above 11.2 GPa and then to a tetragonal $I4/mmm$ structure above 45.5 GPa. However, Gao and Wang *et al.*[33] proposed that the 1*T*-$HfSe_2$ undergoes a phase transition from the trigonal $P\bar{3}m1$ to a hexagonal $P6_3/mmc$ phase near 24 GPa. Compared to the HfS_2 and $HfSe_2$, we note that the high-pressure behavior of 1*T*-$HfTe_2$ has been much less studied except for some fundamental parameters. Until now only a supposed high-pressure marcasite-type structure was proposed for 1*T*-$HfTe_2$ above 12 GPa deduced from the power XRD.[11] However, a full structure determination of the high-pressure phase for 1*T*-$HfTe_2$ was not completely characterized due to the poor quality of the XRD patterns as the authors said. To date, there have been no confirmed reports of pressure-driven structural phase transitions and the resulting electronic properties of 1*T*-$HfTe_2$ that are the aim of this work. It is of great significance to explore new high-pressure phases and special properties of 1*T*-$HfTe_2$, especially for the study of other layered transition metal ditellurides. To settle these points, we have systematically searched the high-pressure structures of $HfTe_2$ up to 50 GPa using the swarm intelligence crystal structure search technique.[34] Two high-pressure monoclinic $C2/m$ and hexagonal $P\bar{6}2m$ phases with three-dimensional (3D) structural framework are uncovered above 3.6 GPa and 9.6 GPa, respectively. The structural features and related electronic properties in comparison with the ambient-pressure trigonal $P\bar{3}m1$ phase are thus studied in detail.

2. Computational methods

A systematic crystal structure search at various pressures points (0 GPa, 5 GPa, 15 GPa, 25 GPa, and 50 GPa) is carried out using the prevalent developed crystal structure analysis by particle swarm optimization (CALYPSO) code[35–37] with 1–4 formula units (f.u.) in the simulation cell. In the process of crystal structure search, 40 structures are generated in each generation, 60% of which are obtained by PSO operation of crystal structures with lower enthalpies in the previous generation, and the remaining 40% are generated randomly, so as to ensure the diversity of crystal structures in each generation. The structure search simulation was terminated after generating $\sim$ 1200 structures ($\sim$ 30 generations). The effectiveness of this swarm intelligence software had been well verified in various systems.[38–43] The energetically stable candidates searched by CALYPSO code were then completely relaxed and their enthalpies, phonons, and electronic structures were calculated using the first-principles calculations. The Vienna *ab initio* simulation package (VASP)[44] was applied here by adopting the projector-augmented wave (PAW)[45] ion–electron potentials and the Perdew–Burke–Ernzerhof (PBE)[46,47] exchange–correlation functional. The cutoff energy of 500 eV for the plane-wave expansions and dense *k*-point with grid density of $0.03 \times 2\pi$ Å^{-1} (Monkhorst–Pack scheme)[48] in the Brillouin zone integration were used to ensure the total energies well converged to be better than $\sim$ 1 meV/atom. The semiempirical DFT-D3 Grimme's method[49] for the vdW corrections was adopted in the structural optimizations. The Heyd–Scuseria–Ernzerhof (HSE06) function[50] and the PBE with spin–orbit coupling (SOC) were selected for the electronic band structure calculations. Phonon dispersions were calculated using the finite-displacement method, as implemented in the PHONOPY code.[51]

3. Results and discussion

At ambient conditions, the experimentally trigonal $P\bar{3}m1$ phase (Fig. 1(a)) for $HfTe_2$ is well reproduced in our variable-cell structural searches, validating our method adopted here. In Fig. 1(a), each Hf atom is bonded to six Te neighbors to form a $HfTe_6$ octahedron in the Te–Hf–Te sandwich layers, the ambient-pressure $P\bar{3}m1$ phase thus can be viewed as the stacking of the edge-sharing $HfTe_6$ octahedra along the *c*-axis. Through structural relaxations, the calculated lattice parameters of $P\bar{3}m1$ phase are in excellent agreement with the experimental data[11] as shown in Table 1. Due to the weak vdW interactions between the Te–Hf–Te sandwich layers in the $P\bar{3}m1$ phase, the application of relatively low pressure can easily squeeze the interlayer spacing and lead to structural transformation. As expected, our swarm intelligence searches at 5 GPa identified an energetically preferable monoclinic $C2/m$ phase (4 f.u./cell) [see Fig. 1(b)], in which each Hf atom is coordinated with eight Te atoms, forming an irregular $HfTe_8$ hendecahedron. Here, it should be noted that all atoms occupy various crystallographic 4*m* sites in this predicted $C2/m$-$HfTe_2$, which is different from the previously reported high-pressure $C2/m$ structures for $TiTe_2$[52] and $HfSe_2$.[32] At higher pressure points of 15 GPa, 25 GPa, and 50 GPa, our structure searches discover a new stable hexagonal $P\bar{6}2m$ structure (3 f.u./cell) [Fig. 1(c)] containing the building block of irregular $HfTe_9$ tetrakaidecahedron. This structure is analogous to that of a typical Fe_2P compound, which was also the high-pressure phase of $TiTe_2$ predicted in a recent theoretical work.[52] As an intriguing crystal structure, this Fe_2P-type phase is already regarded as a universal high-pressure structure in some TM dioxides, such as TiO_2, ZrO_2, VO_2, etc.[53–55] Meanwhile, two tetragonal high-pressure competitive candidates of $P4/mmm$ and $I4/mmm$ structures are discovered, among which the $I4/mmm$ structure has been experimentally determined in the $HfSe_2$.[32]

Table 1. Structural information for $HfTe_2$ within different structures, including space groups, lattice parameters, and Wyckoff positions.

Pressure (GPa)	Space group	Lattice parameter (Å)	Wyckoff position
0	$P\bar{3}m1$	$a=b=3.883$; $c=6.580$	Te: 2*d* (1/3, 2/3, 0.772)
		$\alpha=\beta=90°$; $\gamma=120°$	Hf: 1*b* (0.0, 0.0, 0.5)
0[11]	$P\bar{3}m1$	$a=b=3.911$; $c=6.649$	Te: 2*d* (1/3, 2/3, 0.734)
		$\alpha=\beta=90°$; $\gamma=120°$	Hf: 1*b* (0.0, 0.0, 0.5)
7	$C2/m$	$a=10.739$; $b=3.745$; $c=9.655$	Te: 4*m* (0.210, 0.0, 0.118)
		$\alpha=\gamma=90°$; $\beta=133.617°$	Te: 4*m* (0.102, 0.0, 0.450)
			Hf: 4*m* (0.541, 0.0, 0.192)
20	$P\bar{6}2m$	$a=b=7.810$; $c=3.463$	Te: 3*g* (0.279, 0.0, 0.5)
		$\alpha=\beta=90°$; $\gamma=120°$	Te: 3*f* (0.0, 0.617, 0.0)
			Hf: 2*d* (1/3, 2/3, 0.5)
			Hf: 1*a* (0.0, 0.0, 0.0)

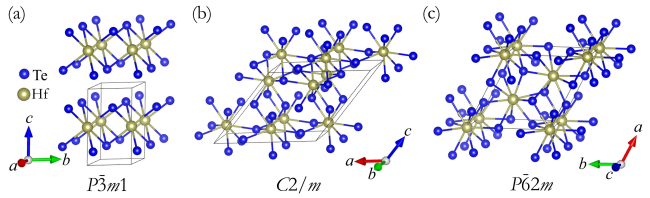


Fig. 1. Crystal structures of (a) $P\bar{3}m1$, (b) $C2/m$, and (c) $P\bar{6}2m$ phases. Large and small balls represent the Hf and Te atoms, respectively.

We show in Fig. 2(a) the calculated enthalpy difference curves (relative to $P\bar{3}m1$) for various predicted structures of $HfTe_2$ under pressure. Here, the earlier proposed marcasite-type structure for $HfTe_2$ and experimental $C2/m$-$TiTe_2$ are not shown due to their higher enthalpy values. It is confirmed from the Fig. 2(a) that the ambient-pressure $P\bar{3}m1$ phase firstly transforms to the $C2/m$ phase after 3.6 GPa, and then, at 9.6 GPa, the $C2/m$ phase transforms to the dense hexagonal $P\bar{6}2m$ phase. Meanwhile, Table 1 lists the detailed lattice constants and atomic positions for three phases at their energetically stable pressure points for further study. Figure 2(b) plots the pressure dependence of the volume per f.u. for each phase along with the experimental data for the $P\bar{3}m1$.[56] Firstly, the calculated volume per f.u. for the $P\bar{3}m1$ phase under pressure accords well with the previous experimental data. Secondly, one can see that these two structural changes of $P\bar{3}m1 \rightarrow C2/m$ and $C2/m \rightarrow P\bar{6}2m$ are all first order demonstrated by the pronounced volume reduction of 7.6% and 4.6%, respectively. In Fig. 1, the formations of high-pressure 3D $C2/m$ and $P\bar{6}2m$ structures can be viewed as the significant shortening of Te–Te interlayer distance and the drastic distortions of $HfTe_6$ octahedra layers in the ambient-pressure $P\bar{3}m1$ structure under increasing compressions. Also, the coordination number of Hf atom increases from six in $P\bar{3}m1$ to eight in $C2/m$ and then to nine in $P\bar{6}2m$ structure at the phase transition process as displayed in Fig. 2(b). We have computed the phonon dispersion curves of $C2/m$ and $P\bar{6}2m$ structures at 9 GPa and 30 GPa and no imaginary phonon frequency is detected in the first Brillouin zone (see Fig. S1), confirming the lattice dynamical stabilities of these two high-pressure phases. Also, both $C2/m$ and $P\bar{6}2m$ phases are mechanically stable by the fact that their calculated single elastic constants (Table S1) satisfy the elastic stability criteria of monoclinic and hexagonal systems,[57] respectively.

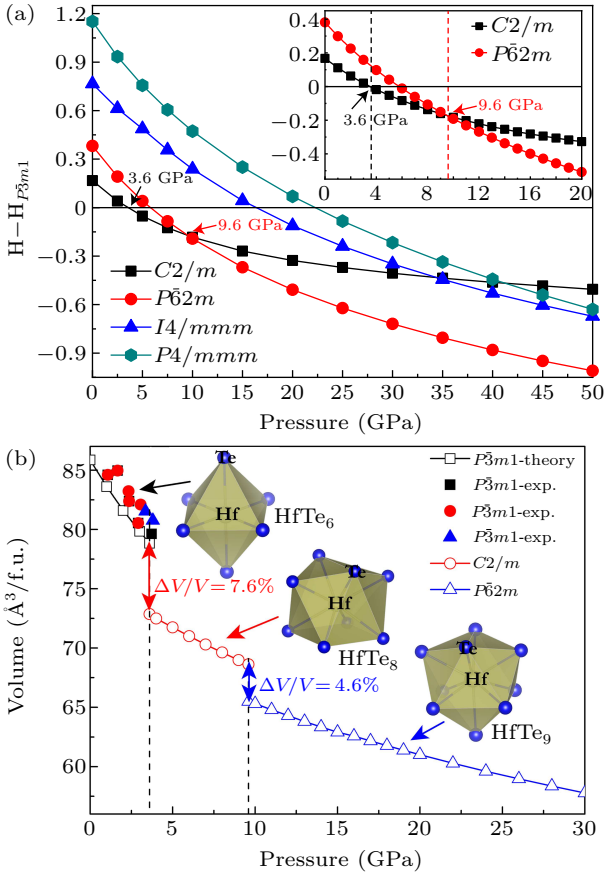


Fig. 2. (a) Enthalpy difference curves (relative to $P\bar{3}m1$) for $HfTe_2$ and (b) the pressure dependence of the volume per f.u. for each structure along with the experimental data for the $P\bar{3}m1$ phase.

X-ray diffraction is a typical technique for determining the crystal structure of solid and a recent experiment has given a well x-ray diffraction pattern of the $P\bar{3}m1$ phase at 0 GPa.[11] To better assist the high-pressure crystal structure characterization in further experiments, we here simulate the power x-ray diffraction patterns of the $P\bar{3}m1$ at 0 GPa, $C2/m$ at 7 GPa, and $P\bar{6}2m$ at 20 GPa in Fig. 3. The Cu-$K\alpha_1$ radiation wavelength is adopted here in keeping with previous

experiment.[11] From the Fig. 3, the simulated main peaks of $P\bar{3}m1$ at ambient pressure match very well with the available experimental data, verifying the reliabilities of the calculated x-ray diffraction patterns of the $C2/m$ and $P\bar{6}2m$ phases.

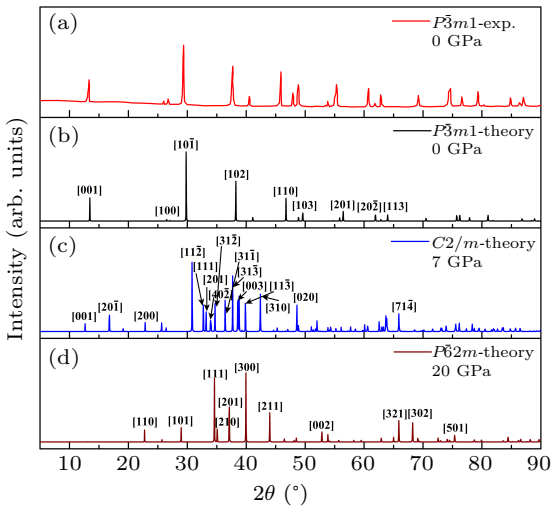


Fig. 3. Panels (a) and (b) are simulated and experimental power XRD patterns of the $P\bar{3}m1$ phase at 0 GPa, (c) the simulated power XRD patterns of $C2/m$ phase at 7 GPa and (d) $P\bar{6}2m$ phase at 20 GPa.

Energy band structures of three phases at the selected pressures using the PBE, PBE + SOC and HSE06 methods are illustrated in Fig. 4 to show the evolution behaviors of their electronic structures. For each phase, it can be seen that the calculated energy band dispersions around the Fermi level (E_F) do not differ significantly between the PBE and PBE + SOC methods. The ambient $P\bar{3}m1$ phase shows a semimetallic behavior [Fig. 4(a)] with the coexisting one electron and two hole bands crossing the E_F. In more detail, as shown in Fig. 4(b), the upper valence band (VB) mainly composed by Te-p orbitals reaches up to and crosses the E_F at Γ and A points forming hole pockets. Contrarily, the conduction band which is mainly dominated by the Hf-d orbitals dips below the E_F to form electron pockets around the L points. 3D Fermi-surface pieces of the $P\bar{3}m1$ phase in Fig. 5(a) are found to be mainly located along the high-symmetry directions in the first Brillouin zone (BZ). In Fig. 4(c), the predicted $C2/m$ shows a clear metallic character originating from the Te-p and Hf-d orbitals along $\Gamma \rightarrow Y$ and $B \rightarrow D$ directions [Fig. 4(d)], corroborating well with the 3D Fermi-surface pieces presented in Fig. 5(b). Compared to the $P\bar{3}m1$ phase, more overlap between the Te-p and Hf-d orbitals is found near the E_F due to the strengthening of Te–Te interlayer coupling and the disappearance of interlayer spacing in $C2/m$ phase. A weak band overlaps in Fig. 4(e) and 3D Fermi-surface plots in Fig. 5(c) imply that the uncovered high-pressure $P\bar{6}2m$ phase is also a semimetal, demonstrated by the traversing of the E_F of electron (along the $\Gamma \rightarrow A$ directions) and hole (at K points) states. However, compared to the $P\bar{3}m1$ phase, both electron and hole states are mainly dominated by the Hf-d orbitals in high-pressure $P\bar{6}2m$ phase [Fig. 4(f)]. It should be noted that to a certain extent, the evolution behavior of electronic structure for $HfTe_2$ in Fig. 4 is consistent with the change of resistivity under compression in the previous experiment.[58] However, no evidence of any related structural phase transition is found in that experimental work, either by x-ray or electron diffraction.

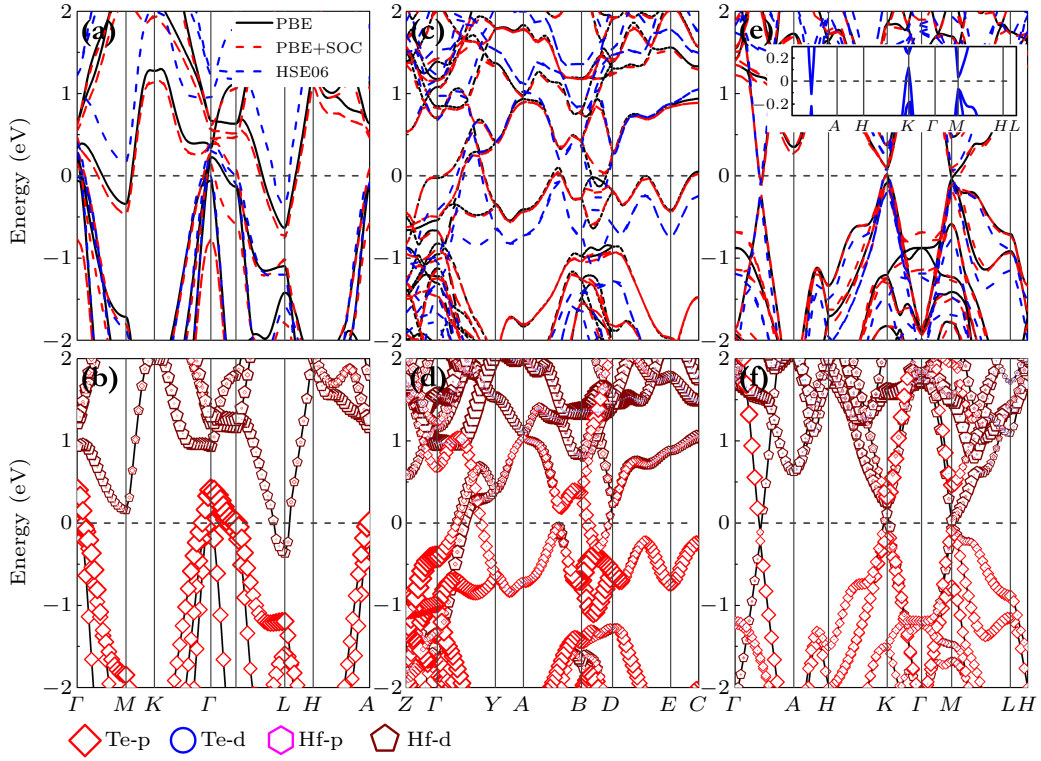


Fig. 4. (a) and (b) Total and orbital-decomposed band structures of $P\bar{3}m1$ phase at ambient pressure , (c) and (d) $C2/m$ phase at 7 GPa, and (e) and (f) $P\bar{6}2m$ phase at 20 GPa.

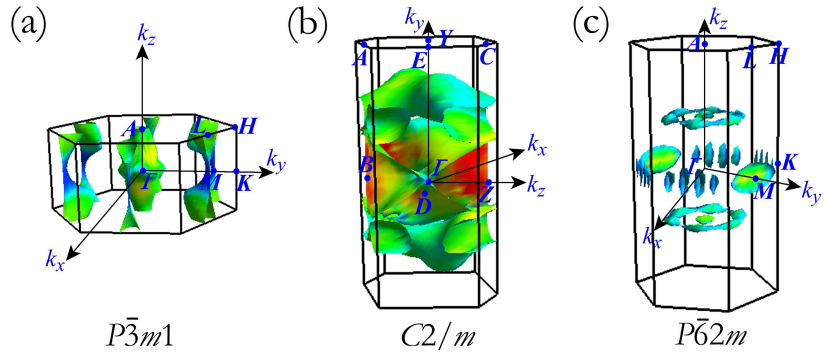


Fig. 5. The 3D Fermi-surface representations of (a) $P\bar{3}m1$ phase at ambient pressure, (b) $C2/m$ phase at 7 GPa, and (c) $P\bar{6}2m$ phase at 20 GPa.

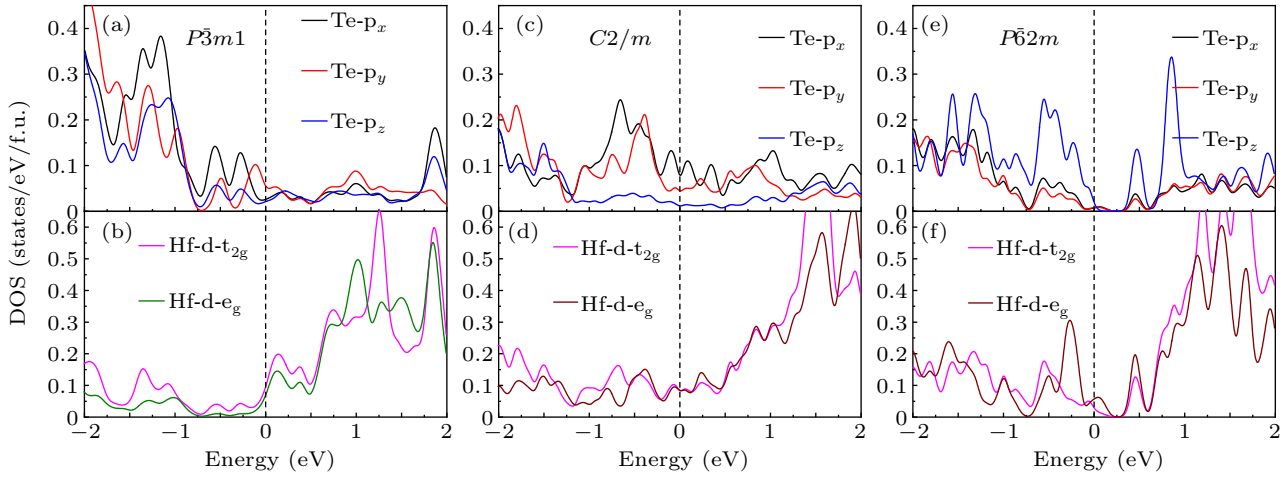


Fig. 6. (a) and (b) Atom-projected DOS of $P\bar{3}m1$ phase at ambient pressure, (c) and (d) $C2/m$ phase at 7 GPa , and (e) and (f) $P\bar{6}2m$ phase at 20 GPa.

The atom-projected electronic density of states (DOS) for Te-p and Hf-d orbitals (doubly degenerate states $e_g(d_{z^2}, d_{x^2-y^2})$ and triply degenerate ones $t_{2g}(d_{xy}, d_{xz}, d_{yz})$) in three phases at HSE06 level are shown in Fig. 6. Meanwhile, the 3D partial charge density distributions of each phase in the energy region of -1 eV to E_F are presented in Fig. 7. Inspection of the electronic DOS in Fig. 6(a) suggests that the Te-p orbital electrons in the $P\bar{3}m1$ phase occupy a larger portion of electronic DOS near the E_F, consisting with the calculated partial charge density distributions in Fig. 7(a) and implying more charge transfer from Hf to Te atoms. From Fig. 6(a) to Fig. 6(c), the contributions of Hf-d orbitals to bonding states near the E_F increase gradually from $P\bar{3}m1$ to $P\bar{6}2m$ phase, coinciding well with the 3D partial charge density distributions in Fig. 7. Compared to the ambient-pressure $P\bar{3}m1$ phase in Fig. 6(a), the increased covalent interactions of Te-p and Hf-d orbitals are revealed by the orbital hybridizations between Te-p$_y$ and Hf-d-t$_{2g}$ in $C2/m$ [Fig. 6(b) and those between Te-p$_z$ and Hf-d-t$_{2g}$ in $P\bar{6}2m$ [Fig. 6(c)] phases. In addition, a relatively weak covalent interaction of Te–Te in $P\bar{6}2m$ phase can also be found from the orbital hybridizations of Te-p$_x$ and Te-p$_y$ in Fig. 6(c). The similar case (the weak Se–Se covalent bonding behavior) has been reported in the high pressure structure of $HfSe_2$.[32] Previous studies[59–61] have suggested that the increased hybridization effect could allow all valence electrons to participate in bonding, thus allowing E_F to reach a valley position conducive to structural stability, separating into bonding and antibonding states (called pseudogap). Thus, a typical feature of the electronic DOS of the $P\bar{6}2m$ phase is the presence of a sharp valley around the Fermi energy, which is the boundary between bonding and antibonding states. Finally, we analyze the charge density topology of $HfTe_2$ under pressure through Bader charge analyses,[62] and the pressure dependence of Bader charge transfers from Hf to Te atom in each phase within its stable pressure range is shown in Fig. 8. A significant charge transfer of $\sim 1.601e$ from Hf to Te in the $P\bar{3}m1$ phase at ambient pressure is shown in Fig. 8, as described in the distributions of orbital-decomposed DOS in Fig. 6(a). Moreover, with the continuous increase of pressure, the value of Hf→Te charge transfer decreases in each phase, resulting in an enhanced covalence of high-pressure structures.

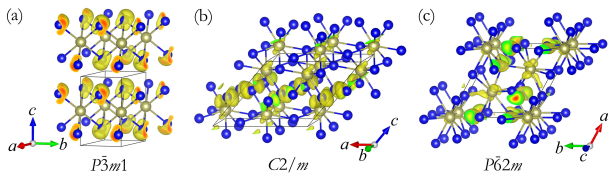


Fig. 7. The 3D partial charge density distributions of (a) $P\bar{3}m1$, (b) $C2/m$, and (c) $P\bar{6}2m$ phases at the energy region of -1 eV to E_F.

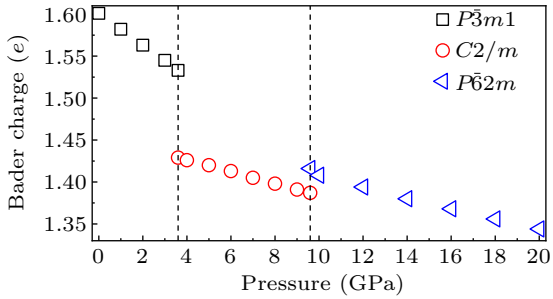


Fig. 8. Pressure dependence of Bader charge transfer from Hf to Te atom of each phase at its stable pressure range.

4. Conclusion

We have extensively explored the high-pressure crystal structures of 1T-$HfTe_2$ up to 50 GPa using the CALYPSO code in conjunction with the first-principles calculations. Two structural transformations have been determined in the compressed $HfTe_2$ which undergoes from the ambient layered and six-fold 1T structure to monoclinic eight-fold coordinated $C2/m$ structure at 3.6 GPa, and then into the hexagonal nine-fold coordinated $P\bar{6}2m$ structure at 9.6 GPa. The result of the pressure dependence of the volume shows that both two structural transitions are first order followed by distinct volume collapses. Analyses of crystal and electronic structures suggest that these transitions are caused by the increased interlayer coupling accompanied by the formation of Te–Te covalent bonding between the interlayer and the strengthening of Hf–Te covalent bonding at high pressure. The obtained findings will extend the high-pressure phase diagram of 1T-$HfTe_2$ and provide valuable insights for other TMDS in further experiments.

Acknowledgments

Project supported by the National Natural Science Foundation of China (Grant No. 11964026) and the Natural Science Basic Research Plan in Shaanxi Province of China (Grant Nos. 2023-JC-YB-021, 2022JM-035, and 2022JQ-008).

References

[1] Mak K F, Lee C, Hone J, Shan J and Heinz T F 2010 *Phys. Rev. Lett.* **105** 136805
[2] Rossnagel K 2011 *J. Phys.: Condens. Matter* **23** 213001
[3] Wang Q H, Kalantar-Zadeh K, Kis A, Coleman J N and Strano M S 2012 *Nat. Nanotechnol.* **7** 699
[4] Qian X, Liu J, Fu L and Li J 2014 *Science* **346** 1344
[5] Ali M N, Xiong J, Flynn S, *et al.* 2014 *Nature* **514** 205
[6] Choi W, Choudhary N, Han G H, Park J, Akinwande D and Lee Y H 2017 *Mater. Today* **20** 116
[7] Wang Y Y, Guo P J, Xu S, Liu K and Xia T L 2020 *Phys. Rev. B* **101** 035145
[8] Li Y, Chen H L, Guo Y X, *et al.* 2021 *Photonics Res.* **9** 1039
[9] Cruzado H N, Dizon J S C, Macam G M, *et al.* 2021 *ACS Appl. Electron. Mater.* **3** 1071
[10] Kowalski R A, Nolen J R, Varnavides G, *et al.* 2022 *Adv. Opt. Mater.* **10** 2200933
[11] Mangelsen S, Naumov P G, Barkalov O I, *et al.* 2017 *Phys. Rev. B* **96** 205148
[12] Singh D and Ahuja R 2019 *ACS Appl. Energy Mater.* **2** 6891
[13] Wang D, Zhang X, Guo G, *et al.* 2018 *Adv. Mater.* **30** 1803285
[14] Kang M, Rathi S, Lee I, Lim D, Wang J, Kahn M A and Kim G H 2015 *Appl. Phys. Lett.* **106** 143108
[15] Kang M, Rathi S, Lee I, *et al.* 2017 *Nanoscale* **9** 1645
[16] Youbi Z E, Jung S W, Mukherjee S, *et al.* 2020 *Phys. Rev. B* **101** 235431
[17] Lin J, Du X and Yang G 2019 *Chin. Phys. B* **28** 106106
[18] Yuan H T, Bahramy M S, Morimoto K, *et al.* 2013 *Nat. Phys.* **9** 563
[19] Yuan H T, Wang X Q, Lian B, *et al.* 2014 *Nat. Nanotechnol.* **9** 851
[20] Cao Y, Zhu X T, Zou D F, Sheng W and Xu Y 2022 *J. Phys. D: Appl. Phys.* **55** 475301
[21] Yun W S, Han S W, Hong S C, Kim I G and Lee J D 2012 *Phys. Rev. B* **85** 33305
[22] Zhang Q Y, Cheng Y C and Schwingenschlögl U 2013 *Phys. Rev. B* **88** 155317
[23] Sahoo S, Dutta U, Harnagea L, Sood A K and Karmakar S 2020 *Phys. Rev. B* **101** 014514
[24] Kang D F, Zhou Y Z, Yi W, *et al.* 2015 *Nat. Commun.* **6** 7804
[25] Lin Y C, Dumcenco D O, Huang Y S and Suenaga K 2014 *Nat. Nanotechnol.* **9** 391
[26] Saqib H, Rahman S, Zhao Y S, *et al.* 2021 *J. Phys. Chem. Lett.* **12** 9859
[27] Sun Y, Wu S C, Ali M N, Felser C and Yan B H 2015 *Phys. Rev. B* **92** 161107
[28] Ibáñez J, Woźniak T, Dybala F, Oliva R, Hernández S and Kudrawiec R 2018 *Sci. Rep.* **8** 12757
[29] Grzeszczyk M, Gawraczyński J, Woźniak T, *et al.* 2002 *Acta Phys. Pol. A* **141** 95
[30] Hong M L, Dai L D, Hu H Y, *et al.* 2022 *J. Mater. Chem. C* **10** 10541
[31] Zhang X, Liu B, Liu S, *et al.* 2021 *J. Alloys Compd.* **867** 158923
[32] Tian C, Gao Y P, Tian F B, *et al.* 2022 *Phys. Rev. B* **105** L180506
[33] Rahman S, Saqib H, Liang X, *et al.* 2022 *Mater. Today Phys.* **25** 100698
[34] Wang Y, Lv J, Zhu L and Ma Y 2010 *Phys. Rev. B* **82** 094116
[35] Wang Y, Lv J, Zhu L and Ma Y 2012 *Comput. Phys. Commun.* **183** 2063
[36] Shao X, Lv J, Liu P, *et al.* 2022 *J. Chem. Phys.* **156** 014105
[37] Tong Q, Lv J, Gao P and Wang Y 2019 *Chin. Phys. B* **28** 106105
[38] Miao J Y, Lu Z S, Peng F and Lu C 2021 *Chin. Phys. Lett.* **38** 066201
[39] Ma L, Wang K, Xie Y, *et al.* 2022 *Phys. Rev. Lett.* **128** 167001
[40] Wang Q F, Cui W W, Gao K, *et al.* 2022 *Phys. Rev. B* **106** 054519
[41] Zhong X, Sun Y, Iitaka T, *et al.* 2022 *J. Am. Chem. Soc.* **144** 13394
[42] Wei Q, Yan Y, Jia X, Yan H, Zhang M, Wu Z and Zhou Y 2023 *Phys. Lett. A* **457** 128540
[43] Zhang S, He J, Zhao Z, Yu D and Tian Y 2019 *Chin. Phys. B* **28** 106104
[44] Kresse G and Furthmüller J 1996 *Phys. Rev. B* **54** 11169
[45] Blöchl P E 1994 *Phys. Rev. B* **50** 17953
[46] Perdew J P, Burke K and Ernzerhof M 1996 *Phys. Rev. Lett.* **77** 3865
[47] Perdew J P, Chevary J A, Vosko S H, *et al.* 1992 *Phys. Rev. B* **46** 6671
[48] Monkhorst H J and Pack J D 1976 *Phys. Rev. B* **13** 5188
[49] Grimme S, Antony J, Ehrlich S and Krieg H 2010 *J. Chem. Phys.* **132** 154104
[50] Krukau A V, Vydrov O A, Izmaylov A F and Scuseria G E 2006 *J. Chem. Phys.* **125** 224106
[51] Togo A, Oba F and Tanaka I 2008 *Phys. Rev. B* **78** 134106
[52] Hu K, Lian J C, Zhu L, Chen Q J and Xie S Y 2020 *Phys. Rev. B* **101** 134109
[53] Dekura H, Tsuchiya T, Kuwayama Y and Tsuchiya J 2011 *Phys. Rev. Lett.* **107** 045701
[54] Nishio-Hamane D, Dekura H, Seto Y and Yagi T 2014 *Phys. Chem. Miner.* **42** 385
[55] Xie S Y, Wang L H, Liu F Y, *et al.* 2018 *J. Phys. Chem. Lett.* **9** 2388
[56] Aoki Y, Sambongi T, Takahashi H, Mori N, Levy F and Berger H 1995 *Synth. Met.* **71** 1883
[57] Mouhat F and Coudert F X 2014 *Phys. Rev. B* **90** 224104
[58] Klipstein P C, Guy D R P, Marseglia E A, *et al.* 1986 *J. Phys. C: Solid State Phys.* **19** 4953
[59] Burdett J K, Canadell E and Miller G J 1986 *J. Am. Chem. Soc.* **108** 6561
[60] Vajeeston P, Ravindran P, Ravi C and Asokamani R 2001 *Phys. Rev. B* **63** 045115
[61] Zhang M, Wang H, Wang H, Zhang X, Iitaka T and Ma Y 2010 *Inorg. Chem.* **49** 6859
[62] Bader R F W 1990 *Atoms in Molecules: A Quantum Theory* (Oxford: Oxford University Press)